Primary chemical sequence ultimately determines crystal thickness in segmented all-aliphatic co-polymers

Yaroslav I. Odarchenko[a,b], Denis V. Anokhin[c], David Doblas[a], Martin Rosenthal[c], Jaime J. Hernandez[a], Loic Vidal[a], Niels J. Sijbrandi[d], Ad J. Kimenai[f], Edwin P.C. Mes[f], René Broos[f], Georg Bar[e], Pieter J. Dijkstra[d], Jan Feijen[d], Mikhail Soloviev[b] and Dimitri A. Ivanov[a,c]**

[a]Institut de Sciences des Matériaux de Mulhouse-IS2M, CNRS UMR 7361, 15 Jean Starcky, 68057 Mulhouse, France

[b]School of Biological Sciences, Royal Holloway University of London, TW20 0EX, United Kingdom

[c]Faculty of Fundamental Physical and Chemical Engineering, Moscow State University, GSP-1, Leninskie Gory, 119991 Moscow, Russia

[d]Department of Polymer Chemistry and Biomaterials, MIRA Institute for Biomedical Technology and Technical Medicine, Faculty of Science and Technology, University of Twente, P.O. Box 217, 7500 AE Enschede, The Netherlands

[f]Core R&D, DOW Benelux BV, P.O. Box 48, 4530 AA Terneuzen, The Netherlands

[e]Dow Olefinverbund GmbH, PF 1163, D-06258 Schkopau, Germany

KEYWORDS: Thermoplastic elastomers, bisoxalamides, crystallization, X-ray scattering, Nanocalorimetry

Thermoplastic elastomers (TPEs) are known to exhibit a phase-separated morphology, which depends on their chemical structure and processing. The design of novel TPEs with predefined properties which are also independent of the material thermal history has so far remained a challenge. The focus of this work is on the semicrystalline morphology of all-aliphatic thermoplastic elastomers consisting of alternating polytetrahydrofuran (PTHF) segments and uniform glycine or β-alanine bisoxalamide units. The thickness of the hard-segment crystals was found to be highly monodisperse and independent of the sample thermal history. Using Nanocalorimetry we observed that at cooling rates as high as 12000 °C·s^{-1} the bisoxalamide segments can still crystallize although the crystallization temperature decreases by ca. 26 °C. The surface free energy of the hard-block crystals is found to be extremely low (~18 erg/cm^2), which is likely due to the entropic contribution of soft segments forming tie chains bridging the neighbouring crystals. To investigate the combined effect of crystal orientation and phase transitions simultaneous time-resolved X-ray scattering and mechanical tensile tests were performed. Upon stretching, elastomeric PTHF segments with lengths above 1000 g·mol^{-1} crystallize at ambient temperatures. Under these conditions two main morphologies were observed: at low strains the long axes of the fibril-like crystals were oriented parallel to the flow direction, whereas higher strains caused bisoxalamide crystal fragmentation and changed their preferential direction to the one perpendicular to the drawing direction. The chain tilts in the bisoxalamide crystals were calculated from the characteristic four-spot SAXS patterns and were ~5 to 16° in case of glycine end groups and 24° for alanine and propyl terminal groups. To our

knowledge this is the first work to determine the chain tilt for non-lamellar crystals in the block copolymers.

INTRODUCTION

Recent advances in the design of thermoplastic elastomers stimulated further research into their structure and morphology.[1,2] At service temperatures these materials typically exhibit a phase-separated morphology which depends on the chemical structure, weight fractions and polydispersity of the soft and hard blocks, as well as on preparation conditions such as the sample thermal history. The segmented block copolymers with uniform hard units constitute a special type of TPEs showing fast and nearly complete crystallization. Their morphology is characterized by ribbon-like crystals immersed in a soft-segment matrix.[3,4] Analysis of the thickness of the hard-block crystals is typically based on either DSC data (indirect analysis) or on qualitative analysis of AFM images.[3,5,6] Monodisperse crystals of semicrystalline polymers are rare and only few observations were reported to date.[7–10]

Processing conditions are known to affect crystallinity of thermoplastic elastomers. For example, change in the crystallization temperature during cooling from the polymer melt and structural defects of different nature typically result in crystal size polydispersity.[11–13] Physical properties of semicrystalline polymers are strongly dependent on crystallinity and therefore processing conditions.[14,15] The design of novel TPEs with predefined properties which are also independent of the processing conditions is an important challenge.

Apart from a uniform crystal thickness, structural development during mechanical deformation is also important in the performance of segmented block copolymers. IR spectroscopy studies reveal two main stages in morphological reorganization of copolymers in response to mechanical deformation.[3,6] At low drawing ratios, below the yield point the hard segment chains in the crystals are preferentially oriented perpendicular to the drawing direction. Above the yield point, crystal fragmentation occurs and the hard segments in the crystals reorient along the stretching

axis. Small-Angle X-ray Scattering (SAXS) studies showed that at large deformations the broken lamellae transform into highly stressed nanofibrils consisting of alternating hard and soft segments.[16,17] For some stretched TPEs the four-spot SAXS patterns were recorded. The phenomena was attributed to the formation of a tilted hard-segment morphology and high aspect ratio of the crystals.[16–18] In contrast, for polyolefins like polyethylene (PE) the four-spot SAXS signal was assigned to the tilted-chain morphology in the folded lamellar crystals.[19,20] The chain tilt angle Φ_c reflects the inclination of the polymer chains with respect to the basal crystal surface normal. Originally, the tilt angle was suggested by Peterlin *et al.*[19] from the difference in the long periods for the drawn PE. Later the Φ_c value in single crystal mats was confirmed by X-ray and electron diffraction experiments.[21,22] More recently, an accurate value of 35° for the chain tilt in the bulk PE was measured by our group using microfocus X-ray scattering on bulk samples containing banded spherulites.[23] To our knowledge, the chain tilt in the crystals of phase-separated block copolymers has not yet been reported. The hard block in the TPEs with uniform hard segments is highly crystalline, with the degree of crystallinity approaching 100%. In contrast to the above, its weight content in the copolymers typically does not exceed 25%. Such low weight fraction limits classical structural methods generally used for semicrystalline homopolymers.[14]

In this report, we describe a polymer system for which the crystalline morphology can be defined entirely by the primary chemical sequence. We combined optical microscopy, electron diffraction, *in-situ* stretching and X-ray scattering, temperature-dependent SAXS/WAXS, and Nanocalorimetry measurements to study crystal morphology and crystallization, deformation behaviour, crystal orientation, and phase transitions of hard and soft segments in the segmented block copolymers of poly(ether ester amide)s (PEEA)s.

EXPERIMENTAL SECTION

Samples. Segmented poly(ether ester amide)s (illustrated in Scheme 1) comprising glycine- or β-alanine- extended bisoxalamide hard segments $PTHF_{1000}$-Gly-$OXA_2$2-Gly **(1000Gly2)**, $PTHF_{1000}$-Gly-$OXA_2$4-Gly **(1000Gly4)**, $PTHF_{1000}$-Gly-$OXA_2$6-Gly **(1000Gly6)**, $PTHF_{2000}$-Gly-$OXA_2$6-Gly **(2000Gly6)**, $PTHF_{2900}$-Gly-$OXA_2$6-Gly **(2900Gly6)**, $PTHF_{1000}$-βAla-$OXA_2$6-βAla **(1000Ala6)** and $PTHF_{1100}$-$OXA_2$6 **(1100Oxa6)** were prepared as reported previously.[4,24] The transparent elastic solid films were prepared by quenching a polymer melt in ice or by non-isothermal melt crystallization using a cooling rate of 5 ºC·min^{-1}.

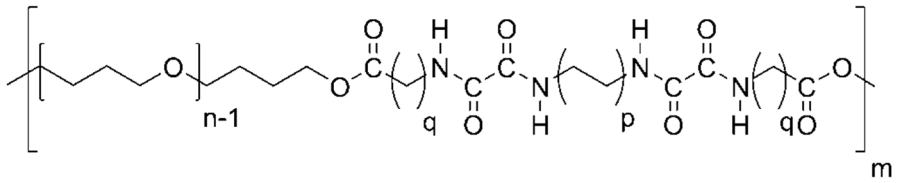

p = 1, q = 1 $PTHF_{1000}$-Gly-$OXA_2$2-Gly (1000Gly2)
p = 2, q = 1 $PTHF_{1000}$-Gly-$OXA_2$4-Gly (1000Gly4)
p = 3, q = 1 $PTHF_{1000}$-Gly-$OXA_2$6-Gly (1000Gly6)
p = 3, q = 1 $PTHF_{2000}$-Gly-$OXA_2$6-Gly (2000Gly6)
p = 3, q = 1 $PTHF_{2900}$-Gly-$OXA_2$6-Gly (2900Gly6)
p = 3, q = 2 $PTHF_{1000}$-βAla-$OXA_2$6-βAla (1000Ala6)

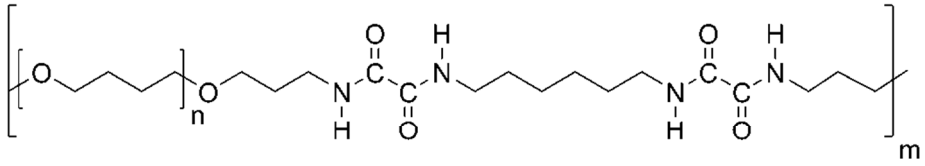

p = 3, q = 0 $PTHF_{1100}$-$OXA_2$6 (1100Oxa6)

Scheme 1. Chemical structures of the studied segmented block copolymers. *p* is the number of ethylene groups between oxalamide units and *q* corresponds to the number of carbon atoms between oxalamide and ester groups.

Polarized optical microscopy (POM). POM observations in transmission mode were carried out using an Olympus BX51 microscope equipped with a digital colour camera (Olympus DP70).

Wide- and Small-Angle X-ray Scattering (WAXS and SAXS). The experiments were conducted on the BM26 beamline of the ESRF (Grenoble, France) using a wavelength of 1.04 Å. The experimental setup comprised 2D detectors (a FReLoN for WAXS and a Pilatus 1M for SAXS). The sample-to-detector distances were chosen to allow recording the signal in the s-range ($s=2\sin\theta/\lambda$, where θ is the Bragg angle) from 0.01 to 0.5 $Å^{-1}$. The modulus of the scattering vector **s** was calibrated using several diffraction orders of silver behenate. The diffraction patterns were collected in transmission geometry. The data reduction and analysis, including geometrical and background correction, visualization, radial and azimuthal integration of the 2D diffractograms, were performed using custom-made routines designed in Igor Pro (Wavemetrics Ltd.).

The crystal thickness L_c was calculated by fitting the form-factor present in the SAXS curves using the following expression:

$$I(s) \propto A + \frac{B}{s^n}\left(\frac{\sin(\pi s L_c)}{(\pi s L_c)}\right)^2 \quad (1)$$

The crystal size was estimated from 1D WAXS profiles using the Scherrer's formula:

$$l_{hkl} = \frac{0.94\lambda}{\Delta\cos\vartheta} \quad (2)$$

Temperature-dependent X-ray measurements were performed using a Linkam heating stage with a temperature precision of 0.1 ºC. The films used in stretching experiments were cut from compression-moulded bars (3x10x1 mm^3). The stress-strain tests were conducted using the

Linkam TST 350 tensile stage equipped with the tensile sensor from 0.01 to 20 N. The deformation rate was 10 $\mu m \cdot s^{-1}$.

Selected-Area Electron Diffraction (SAED). The experiments were carried out with a Philips CM200 transmission electron microscope operated at 200 keV. Calibration of the electron diffraction patterns was performed using graphite. The bisoxalamide-based monomer crystals were prepared by precipitation from toluene on glass slides. After the solvent evaporation, the films were floated off in a 1% wt hydrofluoric acid solution. The samples were subsequently transferred onto gold 400-mesh TEM-grids.

Nanocalorimetry. Thermal analysis was performed using a custom-built Nanocalorimeter based on an instrument described previously.[25,26] Polymer samples were cut out from a film precipitated from a 1% wt solution in chloroform, whereas particles of the corresponding monomers were used without additional purification. All samples were deposited with a micromanipulator on thin suspended silicon nitride membranes of a chip-based sensor XEN-39392 (Xensor Integration, Netherlands) with integrated resistive heaters and thermopiles. Figure S1 in Supporting Information shows a typical sample positioned on the sensor. A custom-built electronic interface was used to apply programmed voltage pulses to the heaters in order to generate heating and cooling ramps with controlled rates. The temperature of the sample was obtained from the voltage of the thermopiles assembled on the sensor. The linear cooling rates used in the experiments were 12800, 6400, 3200, 1600, 800, 400 and 50 $°C \cdot s^{-1}$. The calorimetric curves measured at different cooling rates have been corrected for the time delays associated with each cooling rate. For this purpose, an In micro-particle was ramped in the same conditions and the temperature onset of the crystallization peak was recorded.

RESULTS AND DISCUSSION

Structure of the monomers forming the copolymer hard-block

To get insights into the crystalline structure of the hard segments in poly(ether ester amide)s the Gly-OXA$_2$6-Gly monomer having bisoxalamide moieties separated by an alkyl spacer of six methylene units and capped with glycine terminal groups was examined by optical microscopy, X-ray and electron diffraction.

A typical polarized optical micrograph of the monomer shows a strongly birefringent texture suggesting high crystallinity of the material (Figure 1a). The obtained single crystals for SAED experiments have a pronounced needle-like shape and show preferential growth direction (Figure 1b). The latter is due to the strong intermolecular like-to-like amide-amide hydrogen bonds, which, according to the FT-IR measurements, are formed between the oxalamide groups.[18] The corresponding electron diffraction (ED) pattern is illustrated in Figure 1c. The observed diffraction peaks belong to the [0-21] diffraction zone. These diffraction peaks correspond to a monoclinic unit cell with the following parameters: ***a*** = 5.09 Å, ***b*** = 10.88 Å, ***c*** = 27.73 Å and β=79.6°. The measured and calculated *d*-spacing values extracted from EDs are summarized in Table 1. The peak indices obey the following extinction rules: (0kl) k=2n, (hkl) h+k=2n and (0k0) h,k=2n, which are compatible with the C2 symmetry group. The inter-chain distance along the H-bonds direction derived from the diffraction patterns corresponds to the one known for Nylon 6,2.[27] The ***ac***-projection of the Gly-Oxa$_2$6-Gly monomer crystal is shown in Figure 1d. The unit cell contains 2 molecules. The adjacent molecules form H-bonded sheets in the ***ac***-plane. Importantly, the interplanar spacing values obtained from the X-ray measurements of monomer fiber can be indexed using the data derived from ED analysis (Table S1).

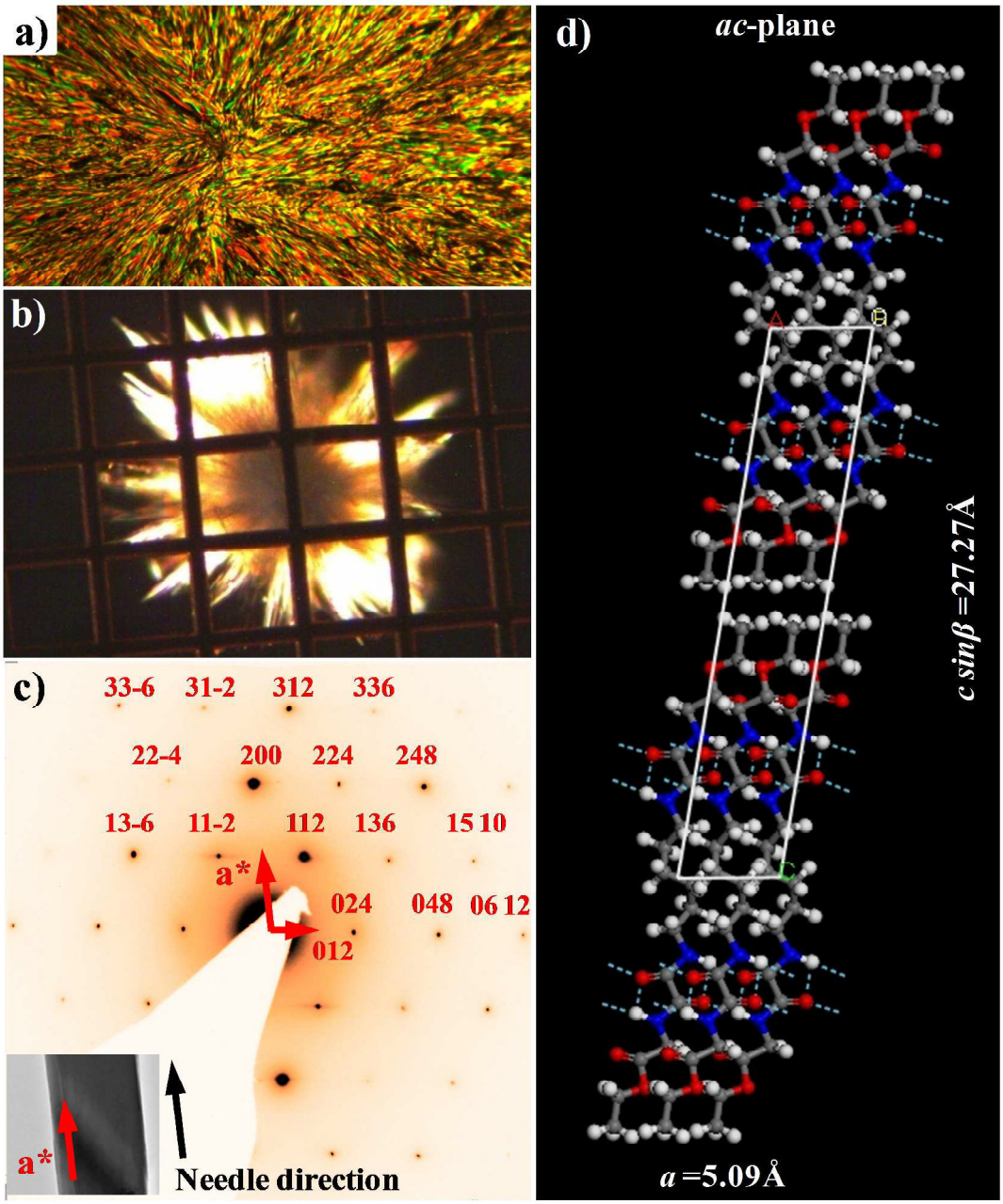

Figure 1. Structure of the Gly-Oxa$_2$6-Gly monomer. POM micrographs of the monomer crystallized between glass cover slips (a) and needle-like crystals deposited on a TEM grid (b). Electron diffraction pattern corresponding to the [0-21] zone and matching TEM-image in correct orientation on the inset (c). Schematic model of the Gly-Oxa$_2$6-Gly crystal (d). The H-bonds are displayed with dotted lines.

Previously, we showed using Raman spectroscopy and X-ray diffraction that the H-bonding direction in the bisoxalamide based monomer is parallel to the ***a***-axis of the crystal.[4] Therefore the indexation of lattice planes was performed assuming that the needle growth axis (H-bond direction) corresponds to the crystallographic ***a**** direction (see Figure 1c,d). The presence of one preferential growth direction is in line with the reported structure of polyoxalamides. Indeed, polyoxalamides with an even number of carbon atoms between the oxalamide groups adopt structures with only one hydrogen bonding direction, whereas the ones with odd spacers exhibit two growth directions of the hydrogen bonds.[27–29]

Table 1. Measured and calculated *d*-spacings (Å) extracted from Selected-Area Electron Diffraction measurements on needle-like crystals of the Gly-Oxa$_2$6-Gly monomer.

h	*k*	*l*	d_{exp}, Å	d_{calc}, Å	Lattice
0	2	4	4.25	4.25	
0	4	8	2.13	2.13	
0	6	12	1.43	1.42	
1	3	-6	2.35	2.36	Monoclinic; C2
1	1	-2	4.12	4.12	N13, c-unique
1	1	2	4.5	4.54	Conditions:
1	3	6	2.62	2.60	(0kl) k=2n
1	5	10	1.67	1.67	(hkl) h+k=2n
2	6	12	1.3	1.30	(0k0) h,k=2n
2	4	8	1.72	1.72	parameters:
2	2	4	2.27	2.27	a=5.09 Å
2	0	0	2.51	2.50	b=10.88 Å
2	2	-4	2.05	2.06	c=27.73 Å
3	3	-6	1.37	1.37	β=79.6°
3	1	-2	1.59	1.60	
3	1	2	1.67	1.67	
3	3	6	1.52	1.51	

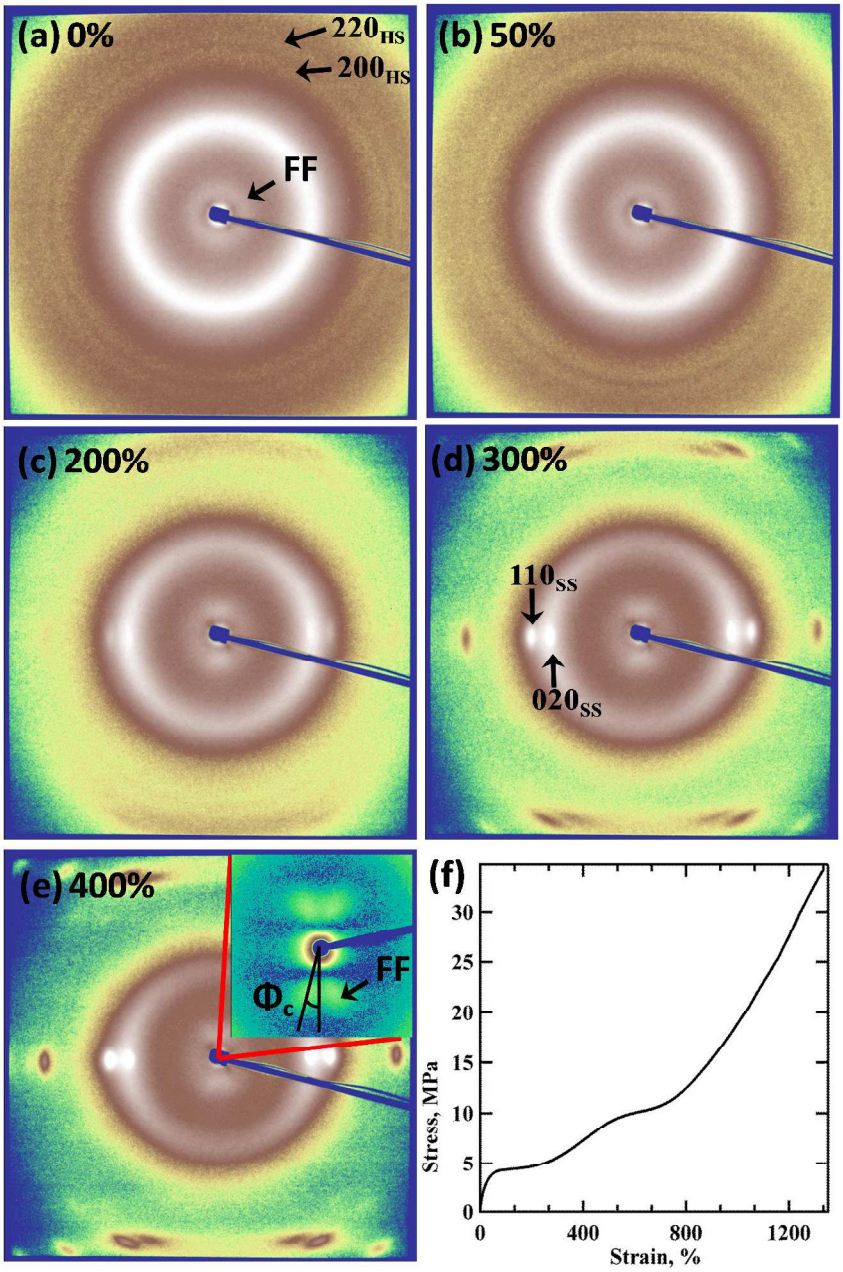

Figure 2. *In-situ* WAXS-stretching experiment of poly(ether ester amide). 2D-WAXS patterns measured during deformation of copolymer **2900Gly6** (a-e). Stress-strain curve for sample **2900Gly6** (f). The inset in the same panel shows a magnified four-spot SAXS pattern corresponding to a strain of 400%. The peaks pertinent to the hard and soft segment crystals are marked with subscripts "HS" and "SS", respectively. The stretching direction is vertical.

Deformation behaviour of poly(ether ester amide)s.

The structure evolution of segmented PEEAs during tensile deformation was studied using *in-situ* X-ray diffraction. Copolymer film samples were drawn at a constant deformation rate of 10 $\mu m \cdot s^{-1}$ and 2D X-ray patterns were recorded simultaneously. Figure 2 shows selected 2D-WAXS patterns for sample **2900Gly6**. At zero deformation the polymer displays isotropic patterns with a strong amorphous halo at about 4.4 Å (Figure 2a), which comes from the amorphous soft block. No traces of the soft block crystals are seen likely because PTHF is not long enough to form stable crystalline nuclei at room temperature. The reflections from the hard segment crystals are largely absent from the diffractograms of copolymer, which is in agreement with our previous results obtained for non-stretched samples.[24] Only two reflections of the bisoxalamide crystals located at 2.48 and 2.30 Å (200 and 220 peaks, respectively) could be detected (Figure 2a). The characteristic feature in the small-angle region can be attributed to the form-factor (FF) generated by the bisoxalamide crystals due to their uniform thickness (Figure 2a). This feature will be described in detail in the following.

At the beginning of a tensile experiment, the non-stretched sample shows isotropic small-angle scattering (Figure 2a), which is ascribed to the random orientation of the hard-segment crystals immersed in the soft block matrix. A schematic model of the non-stretched polymer morphology is illustrated in Figure 3a. At a strain of 50% a faint anisotropy can be seen in the intensity distribution of the Gly-$Oxa_2$6-Gly crystalline peaks and in the PTHF amorphous halo (see Figure 2b). The 200 reflection corresponding to the H-bonds direction exhibits pronounced arcing on the meridian indicating that the hydrogen-bonded sheets become parallel to the elongation direction. Such appearance is typical for orientation of high-aspect-ratio objects in a flow. The

reorganisation of the fibril-like hard block crystals during uniaxial stretching is outlined in Figure 3b. Similar orientation of high-aspect-ratio crystals at the initial stages of deformation (below the yield point) was detected previously using IR spectroscopy by Niesten[6] and Versteegen[3]. The yield point depends on the content and nature of the copolymer segments and is about 100% for copolymer **2900Gly6** with PTHF length 2900 g·mol^{-1} (see Figure 2f). Above the yield point at a strain of 200% sharp crystalline peaks corresponding to the PTHF crystals (reflections 020 and 110) appear on the equator (Figure 2c). The diffraction pattern also shows a diffuse layer line with l=5. These features are a signature of the strain-induced crystallization of the soft block.[6,16,18] Moreover, at the same stage the FF ripple stabilizes on the meridional direction (cf. Figure 2c) indicating that the long axes of the hard-segment crystals become largely oriented perpendicular to the direction of drawing. Upon increasing the strain to 400% more crystalline reflections of the PTHF block become visible and their relative intensity increases (Fig. 2d-e). These crystalline peaks are indexed using monoclinic unit cell of the PTHF with the following lattice parameters: a=5.61Å, b=8.92Å, c=12.25Å and β=134.3°.[30] The experimental and calculated *d*-spacings of the PTHF lattice are given in Table S2.

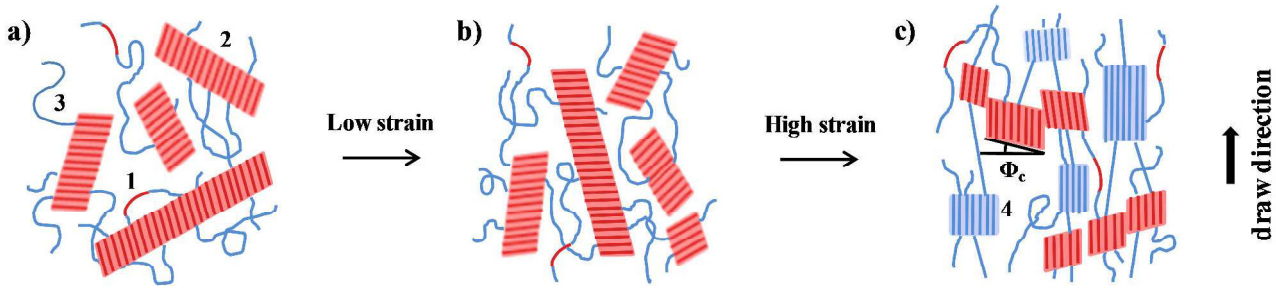

Figure 3. Schematic model of structural changes in PEEAs with uniform hard segments during uniaxial deformation. The non-stretched structure (a); the structure formed below the yield point (b); the structure formed above the yield point (c). The following morphological features are

highlighted: 1 - hard block segment; 2 - hard block crystal; 3 - soft block segment; 4 - soft block crystal; 5 - chain tilt angle Φ_c.

At high deformations (up to 450%) the 200 and 220 reflections of the hard block crystals are typically very weak compared to the PTHF reflections, this makes them almost unobservable in the diffractograms. However, on heating the oriented films above the melting temperature of the PTHF crystals the 200 and 220 crystalline reflections of the bisoxalamide segments become more prominent. For this reason, accurate determination of the bisoxalamide chain orientation was conducted at elevated temperature. This is exemplified in Figure 4 for copolymer **2900Gly6**, which was first stretched to 200% and then heated to 80°C, a temperature chosen to ensure the PTHF crystals melting.[6] The hard-segment 200 and 220 reflections are located on the equator indicating that the bisoxalamide crystal stems are preferentially oriented along the stretching direction (Figure 4a). This is supported by the presence of the strong FF signal positioned approximately on the meridian (Figures 2c-e and Figure 4a).

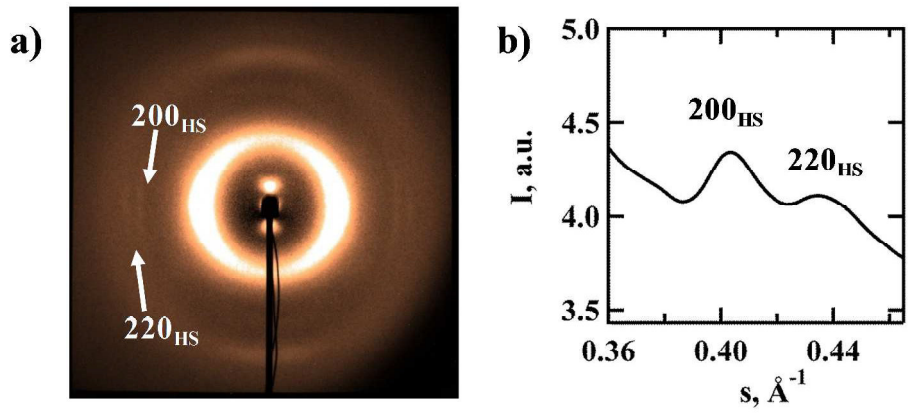

Figure 4. Detection of the hard-block crystals in stretched poly(ether ester amide)s **2900Gly6** above melting temperature of the soft-block. 2D-WAXS pattern of **2900Gly6** stretched to 200%

deformation and heated to 80 °C (a) and corresponding equatorial section showing two peaks corresponding to the hard segment crystals (b).

A highly oriented PEEA microstructure is depicted in Figure 3c, which shows two types of non-folded crystals formed by the PTHF and bisoxalamide segments connected by taut PTHF chains. For both crystal populations the stems are oriented along the direction of drawing. Beyond the yield point, a different deformation mechanism sets in resulting in fragmentation of the hard-block crystals and leading to a drastic change in their orientation. Such phenomenon was observed previously using only spectroscopic measurements for co-poly(ether-urea)s[3] and segmented copolymer with uniform aromatic untis[6]. In this work we examined the orientation of the hard segment crystals using simultaneous SAXS/WAXS/tensile measurements for the first time. This approach to the analysis of structural changes in PEEAs was viable due to both the crystalline reflections in the wide-angle region and the FF signal in the small-angle region pertinent to the bisoxalamide crystals. The hard segment crystals act as physical cross-links between the soft-block chains ensuring mechanical properties of the material at high temperature, this is also corroborated by the reflections from the bisoxalamide crystals (Figure 4b).

Crystal structure of the stretched poly(ether ester amide)s.

Comparing the highly oriented morphologies of the PEEAs with different PTHF lengths might help to better understand the role of the soft segments in the structure formation of TPEs. We therefore compared the 2D WAXS patterns of the stretched PEEA films with 1000, 2000 and 2900 $g \cdot mol^{-1}$ soft segments containing the Gly-$Oxa_2$6-Gly monomer (Figures 5b-d). For PEEAs

1000Gly6 and **2000Gly6** with short PTHF blocks of 1000 and 2000 respectively, the reflections of the hard-segment crystals are visible on the diffractograms of oriented samples even at room temperature. The peaks corresponding to the bisoxalamide unit cell can be clearly seen on the equator at 200 and 220 (Figures 5b-c). In the extruded bisoxalamide monomer fibers both peaks are positioned on the meridian having a significant azimuthal spread (Figure 5a). The difference in orientation of hard-segment crystals and monomer crystals is likely because of the different mechanisms of the molecular orientation during extrusion. For the polymers stretched to high strains, the H-bonds (***a***-axis) in the hard-block crystals are oriented perpendicular to the drawing direction. Such orientation is opposite to that of the extruded monomer fibers for which the beta-sheets are oriented along the extrusion direction (the fiber axis direction indicated in Figure 5a). This is probably because the hydrogen bonds are already present in the melt[6,31] resulting in fast formation of the H-bonded sheets during the extrusion process.

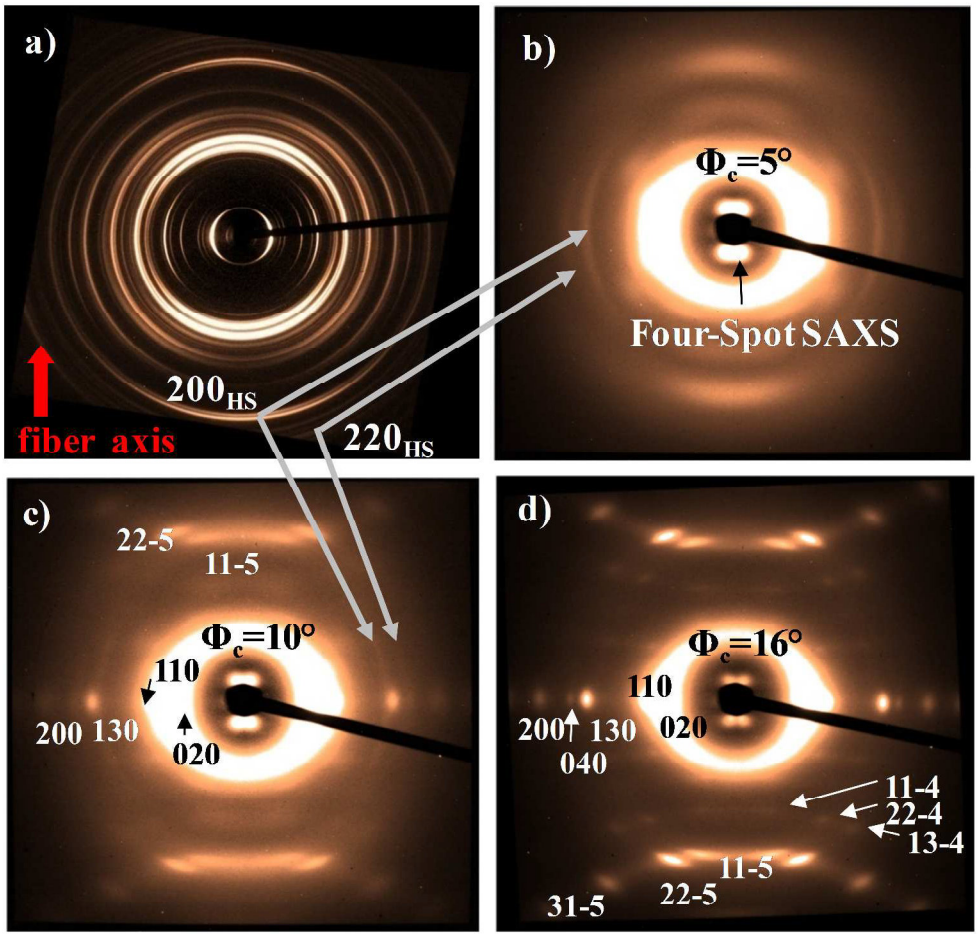

Figure 5. Crystal structure of the stretched poly(ether ester amide)s. 2D-WAXS patterns corresponding to oriented monomer fiber Gly-Oxa$_2$6-Gly (a) and to the corresponding PEEA films with 1000, 2000 and 2900 soft segment lengths (panels b, c and d, respectively). For 2D patterns (b-d) the stretching direction is vertical. The peaks of the hard segment crystals are marked with subscripts "HS".

We conducted temperature-dependent SAXS/WAXS measurements to evaluate differences in the crystallization of soft-block in isotropic and oriented copolymers. The heating ramps for sample **2900Gly6** are shown in Figure 6. The melting temperature T_m of the soft block was monitored by measuring the intensity of the strongest 020 and 110 peaks of PTHF crystals

(Figure 6a-b). The stretched copolymers consistently showed markedly elevated melting temperatures compared to the isotropic material, which is attributed to the stress induced crystallization of the soft segments. For example, the melting temperature increases from -16 to 40 °C for **2000Gly6** and from 3 to 65 °C in case of **2900Gly6** (Table 2). In the previous studies of the pre-strained TΦT-PTHF copolymer with the same soft block lengths a similar but smaller strain effect was detected using conventional DSC[6] . This difference can be attributed to partial relaxation of the polymer chains after the strain was released.

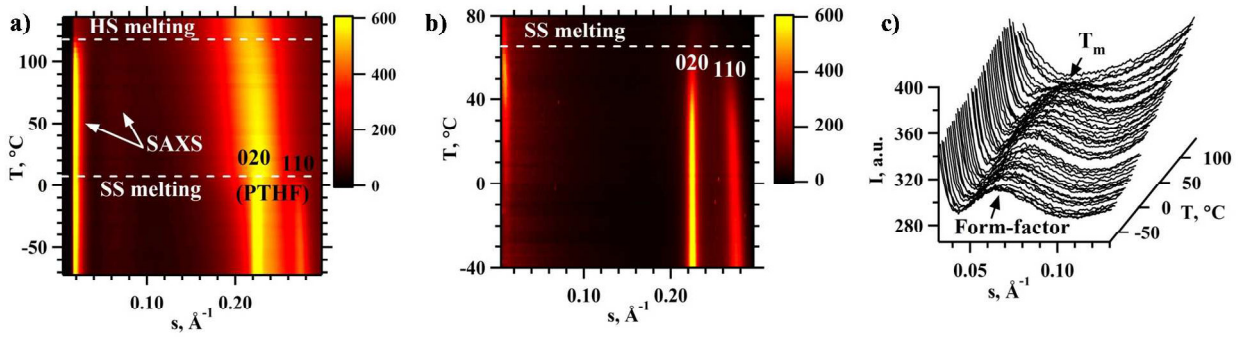

Figure 6. Temperature-dependent SAXS/WAXS measurements for PEEA **2900Gly6.** The scattering patterns measured during a heating ramp at 5 °C/min for the isotropic (a) and oriented (b) copolymers. Magnified SAXS region of the scattering curves in (a) centered on the maximum of the FF (c). The 2D diffractograms were reduced to 1D form using integration within a sector of 5° around the equator for both the isotropic and oriented samples.

Table 2. Characteristics of the PTHF soft segment crystals.

Sample	ISOTROPIC	ORIENTED	
	T_m, °C	T_m, °C	L_c (11-5)*, Å
2000Gly6	-16	40	28

2900Gly6	3	65	54

*crystal thickness values were obtained from the line broadening analysis performed on the 11-5 crystalline reflection

Superposition of the strongest equatorial reflexes with the amorphous halo rules out using 020 and 110 reflexes for determining the PTHF crystal thickness. We have therefore measured the width of the 11-5 peak, which is positioned close to the drawing direction in the diffractograms. The crystal thickness L_c values for the isotropic and oriented copolymers **2000Gly6** and **2900Gly6** are listed in Table 2.

The oriented sample **1000Gly6** with the shortest PTHF segment (1000 g·mol^{-1}) shows only a single equatorial reflection and several diffuse layer lines on the meridian related to a largely disordered chain conformation (Figure 5b). A longer PTHF block with 2000 g·mol^{-1} (**2000Gly6**) crystallizes upon drawing, which resulted in the increase of stress at break by 26% from 22.2 to 28.0 MPa. The stress at break values for the PEEAs samples studied here, were reported previously.[24] For the longer soft block length, i.e. 2900 g·mol^{-1} (**2900Gly6**) the crystal thickness calculated using the Scherrer formula for the 11-5 reflection, increased two fold (from 28 to 54 Å). Such increase may account for an additional increase of stress at break by 22% for **2900Gly6** in respect to **2000Gly6.**

Although the cross-links formed by soft segment crystals may account for the differences in stress at break of the studied polymers, the broad temperature-independent plateau and the Young's modulus in the range of 139 – 170 MPa[24] are mainly determined by the cross-links associated with the hard-segment crystals.[24]

PEEA copolymer morphology and its dependence on the sample thermal history.

We employed small-angle X-ray scattering analysis to estimate the size of the fibril-like crystals. The 1D SAXS profiles of the isotropic PEEAs **1000Gly6**, **2000Gly6** and **2900Gly6** comprising the Gly-Oxa$_2$6-Gly monomer are shown in Figure 7a. The crystal thickness L_c values were calculated from the positions of the form-factor ripple. The FF intensity decreases considerably with increase of the hard-block content from 10.5 to 25.4% by weight. Moreover, the form factor shows the same spacing of 24Å as seen from Table 3 for the different soft segment lengths. This shows that crystal thickness is independent of the soft segment. The exact values of crystal thicknesses are slightly smaller than the projection of the ***c*-**parameter on the ***b**c**-**plane ($c\cdot\sin\beta$) of the corresponding monomer (the inter-layer spacing in the monomer crystals equals 27.3 Å). The difference of 3.3 Å can be accounted for by the exchange of the terminal methyl group by the soft PTHF segment during the melt esterification process.[24] Table 3 lists crystal thickness L_c, long spacing L_B and amorphous layer thickness L_a values for all the samples studied.

Interestingly, for the stretched films, the position of the form-factor ripple shifts to lower angles (Figure 7a and b) indicating that the thickness of the hard block crystals increases along with the improvement of their orientation (Table 3). Given that bisoxalamide crystals are not lamellar, such thickening can be explained by simple "elongation" under the external load, possibly due to the alkyl chains between the oxalamide units adopting a more strained conformation. The latter is supported by the fact that elongation depends on the spacer length *p* and is independent of the soft block length. The strong intensity and the well-defined shape of the FF seen in 1D SAXS curves clearly indicates that the crystal thickness distribution is monodisperse and therefore depends solely on the primary chemical sequence of the copolymers.

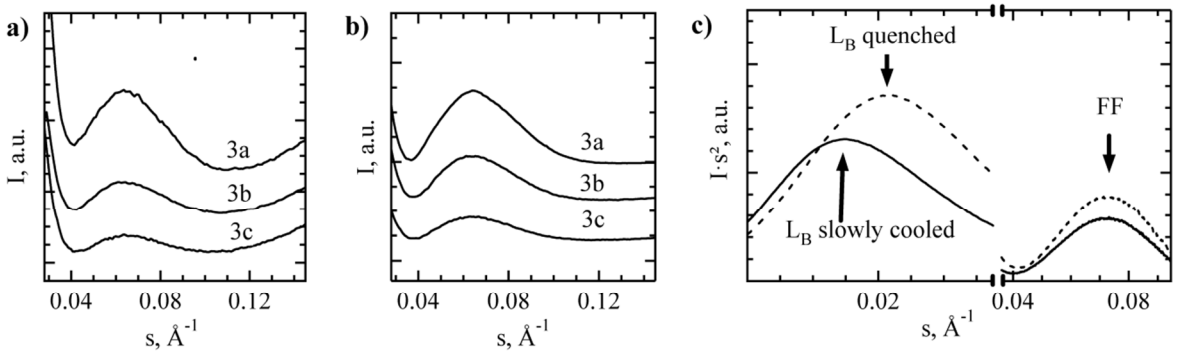

Figure 7. Poly(ether ester amide)s copolymer morphology. SAXS profiles of isotropic (a) and oriented (b) PEEA films. Lorenz-corrected 1D SAXS curves for quenched (dashed line) and slowly cooled (solid line) sample **3a** (c).

Table 3. Long spacing (L_B), crystal thickness (L_c) and amorphous layer thickness (L_a) of isotropic and oriented poly(ether ester amide)s.

Sample	ISOTROPIC			ORIENTED			
	L_B, Å	L_c, Å	L_a, Å	L_B,	L_c, Å	L_a, Å	Φ_c, °
1000Gly2	49.8	14.3	35.5	50.	16.3	34.6	~5
1000Gly4	52.6	17.4	35.2	47.	19.1	28.6	~5
1000Gly6	57.5	24.0	33.5	57.	27.7	29.6	~5
2000Gly6	71.4	24.0	47.4	63.	26.8	36.3	10
2900Gly6	79.0	24.0	55.0	78.	26.8	51.6	16
1000Ala6	73.0	22.9	50.1	50.	23.5	26.9	24
1100Oxa6	75.7	16.5	59.2	57.	18.4	39.3	24

To investigate whether crystal thickness is dependent on the thermal history of the copolymers, we prepared a series of PEEAs samples and subjected them to different thermal treatments. Figure 7c illustrates typical 1D SAXS profiles obtained from quenched and slowly-cooled

isotropic PEEA (**1000Gly6**). The recorded long spacing values L_B are different due to the changes in the microphase separated morphology, whilst the crystal thickness L_c does not vary. The L_B and L_c values for all such samples are reported in Table 4. All the FF comes from the oxalamide crystals and there is no contribution from PTHF crystals, as is evidenced by the heating ramp experiment illustrated in Figure 6 (panels a,c) where the FF values for the hard block are recorded above the melting temperature of the soft block crystals. No SAXS signal is visible in Figure 6b for the heating measurement of the oriented sample due to the fact that the SAXS peaks inclined by 16° with respect to the meridian, which excluded them from the angular sector used for the 2D-to-1D data reduction.

To investigate the rate of polymer crystallisation we used fast Nanocalorimety technique. Nanogram-sized samples were heated above the melting temperature and then cooled at various rates. The Nanocalorimetry curves obtained are reported in Figure S2. The onset of the crystallization temperatures versus the cooling rates are plotted in Figure 8 for Gly-Oxa$_2$2-Gly monomer and polymer **1000Gly2** which incorporates Gly-Oxa$_2$2-Gly as the hard segment. The crystallization temperature onset for the slowest cooling rate of 20 °C·min^{-1} (0.33 °C·s^{-}1) was measured by conventional DSC as reported previously.[24] The crystallization temperature for the monomer was independent on the cooling rate, whereas the same treatment regime resulted in a 26 °C decrease in the crystallization temperature for the corresponding copolymer. For comparison, in the case of homopolymers such as isotactic polypropylene (iPP) the crystallization process is bypassed by formation of the so-called smectic mesophase at cooling rates higher than 160 °C·s^{-1}.[32] As far as polyamides are concerned, a complete vitrification of polyamide-6 was reached for cooling rate above 150 °C·s^{-1}.[33] This shows that the crystallization process in the studied segmented copolymers is extremely fast. One of the possible explanations

can be the existence of the H-bonds in the polymer melt, which was observed previously for the segmented copolymers with uniform aramid and tetra-amide units.[6,34]

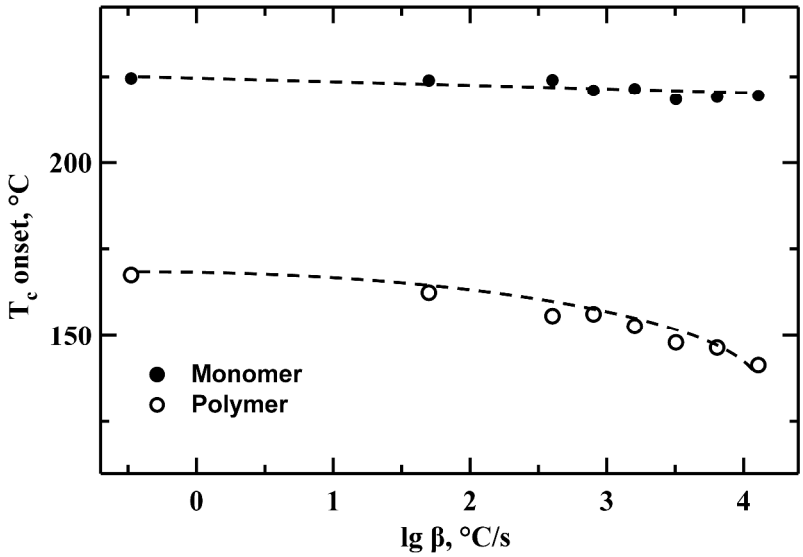

Figure 8. Crystallization temperature onset versus cooling rate for Gly-Oxa$_2$2-Gly monomer and polymer **1000Gly2**. Horizontal axis shows crystallization temperature onset and vertical axis indicates logarithm of cooling rate β.

Table 4. Long spacing (L_B) and crystal thickness (L_c) for slowly-cooled down and quenched isotropic samples of segmented poly(ether ester amide)s.

Sample	L_B, Å		L_c, Å	
	S*	Q**	S*	Q**
1000Gly2	53.3	46.7	14.1	14.0
1000Gly6	65.3	57.0	24.0	23.1
2900Gly6	83.3	75.0	22.4	22.3
1000Ala6	77.8	59.9	21.4	20.6
1100Oxa6	83.9	80.5	15.9	15.7

*slowly cooled to RT at a cooling rate of 5 ºC·min^{-1};
**quenched to ice water.

Chain tilt in the bisoxalamide crystals.

To better understand the chain packing in the hard-segment crystals we first determined the form-factor position on the relevant SAXS patterns. The observed form-factor is not strictly meridional but is split into a clearly pronounced four-spot pattern suggesting a tilt of the hard segment crystalline stems with respect to the crystal basal plane normal (Figure 2e). Although the FF azimuthal position remains constant beyond the yield point during stretching, the calculated chain tilt values from the four-spot SAXS signal differ for various samples (Figure 9). We concluded therefore that these angles represent the inherent feature of the bisoxalamide crystals. The alignment of the PTHF chains, which bridge the bisoxalamide segments, induces all hard block crystals to become inclined with respect to the drawing axis at a fixed angle Φ_c (see Figure 3c). The chain tilt values for all the PEEAs studied are summarized in Table 3. In the present research, the chain tilts Φ_c depend on the hard segment present and are relatively small (~5-16°) for the case of glycine end-group**,** whilst they increases to 24° for segments with alanine and propyl end–groups (Table 3). The formation of a tilted morphology for the urethane-based elastomers has been previously reported by Bonart[18] and Hsiao[16] and was explained in terms of the high aspect ratio of hard-block crystals. However, no correlation between the chain tilt and the packing of the bisoxalamide stem in hard segment crystals was observed or reported until now. From our work it can be concluded that chain tilts for bisoxalamide crystals depend on the nature of the hard-segments.

The occurrence of a chain tilt is accounted for by the necessity to accommodate the chain folds on the disordered fold surfaces. For PE crystals of orthorhombic symmetry the chain tilt of 35° is

likely to be dictated by a large difference (~16.5%) between densities of amorphous and crystalline phases.[23,35] This is also supported by the fact that some (unfolded) paraffins exhibit the same orthorhombic structure but do not have a chain tilt.[36] In contrast to PE, the orthorhombic crystals of polyhydroxybutyrate (PHB) characterized by a density difference with the melt state of only 7% are known to crystallize without chain tilt.[37] The preservation of chain tilt upon drawing is well established.[19] Also in recent simulations of deformation of polyethylene Rutledge *et al*.[38] showed that the chain tilt in the lamella crystals can remain constant during deformation. To the best of our knowledge chain tilt has not been reported for non-lamellar crystals in the segmented block copolymers.

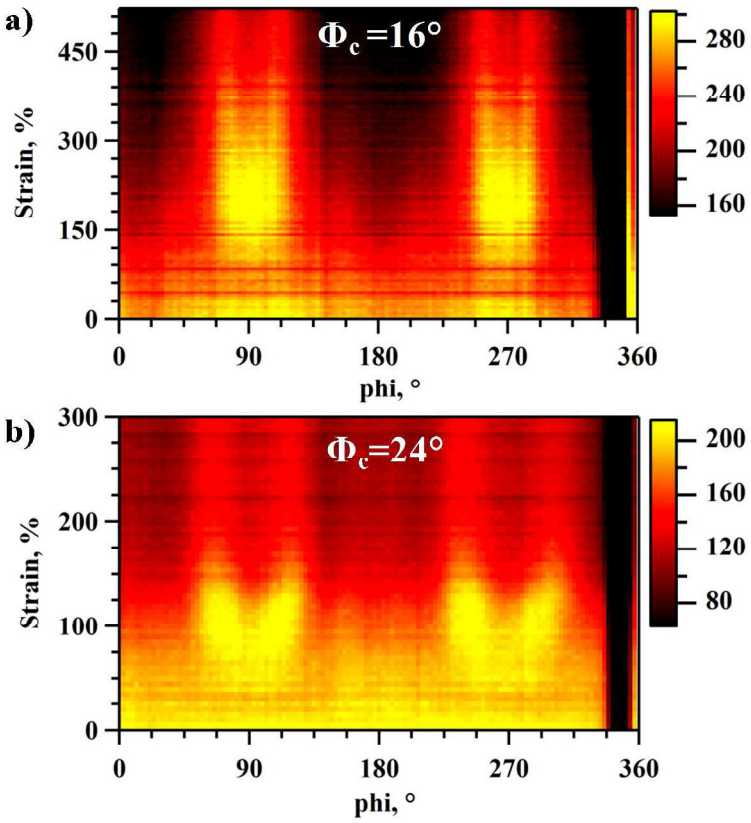

Figure 9. *In-situ* SAXS-stretching experiments of PEEAs. Azimuthal intensity profiles are calculated for samples **2900Gly6** (a) and **1000Ala6** (b) in the s-range between 0.045 and 0.090.

Surface energy of the bisoxalamide crystals.

In our study, we were interested also in the thermodynamics of the high-aspect-ratio bisoxalamide crystals. The melting enthalpy per mole of the bisoxalamide crystals, ΔH, derived from the DSC data (not shown), are given in Figure 10a as a function of the spacer length p. The enthalpy for the bisoxalamide based crystals with the glycine end group **(1000Gly2, 1000Gly4** and **1000Gly6)** does not depend on the spacer length, whereas for the propyl end-group **(1100Oxa6)** and the alanine end-group **(1000Ala6)** the enthalpy varies with the spacer length as much as 30%. That proves that the nature of the segment end-group plays a significant role in stability of crystals.

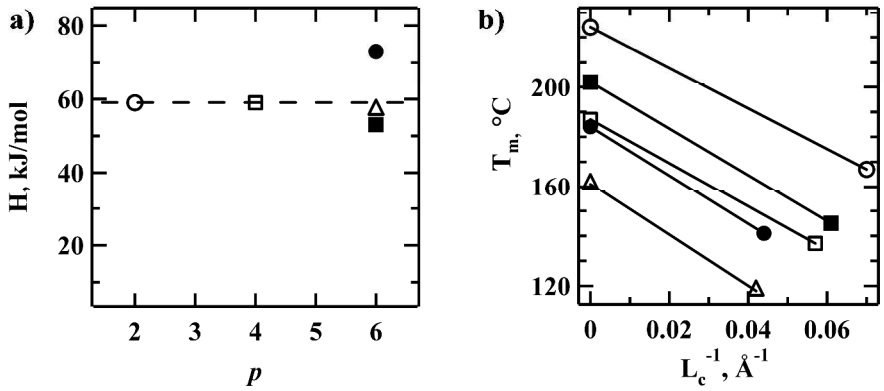

Figure 10. The melting enthalpy per mole of the hard-segment crystals *vs.* spacer length p (a). Gibbs-Thomson plot showing the melting temperature *vs.* reciprocal crystal size (b). All copolymers have a short PTHF segment length of 1000 g·mol^{-1} (polymers **1000Gly2**(○), **1000Gly4**(□), **1000Gly6**(■) and **1000Ala6**(●)) or 1100 g·mol^{-1} (polymer **1100Oxa6**(Δ)).

To calculate the surface energy of the hard-block crystals we used the Gibbs-Thomson equation. It correlates the melting point depression with the crystal thickness as follows:

$$T_m = T_m^0\left(1-\frac{2\sigma_e}{\rho L_c \Delta H_f}\right) \quad (3)$$

Since the exact equilibrium melting temperatures of the compounds is unknown, we have used instead the melting temperature of the corresponding monomers, which form macroscopically thick crystals.[24,39] The melting temperatures of the hard-segment crystals are only 20 °C lower than those of the corresponding monomers. When plotted in the Gibbs-Thomson coordinates, essentially the same slope is observed for copolymers with similar PTHF lengths (Figure 10b). The estimated surface energy σ_e is 18 erg/cm^2, which is relatively low compared to that of conventional homopolymers.[40,41] Moreover since our crystals are needle-like,[39] this can make the efficient energy values even lower. Similar surface energy values were reported previously for nylon 6,6 and were accounted for by a different crystallization mechanism similar to that observed in non-polymeric materials.[42] In the case of PEEA copolymers reported here, such a low value is likely due to the entropic contribution of the soft segments forming tie chains bridging the neighbouring crystals.

CONCLUSIONS

We have applied *in-situ* SAXS/WAXS measurements, electron diffraction, Nanocalorimetry and optical microscopy to study segmented poly(ether ester amide)s and found that crystal size depends solely on the primary chemical sequence. We showed that the thickness of the hard-segment crystals is highly monodisperse and independent of the sample thermal history. The uniform hard segments show similar crystallization behaviour to that of the corresponding bisoxalamide based monomer that crystallize extremely rapidly i.e. at the cooling rate above 12000 °C·s^{-1}. The unit cell of the monomer consisting of a bisoxalamide array with a spacer length of six methylene units and capped with glycine end groups was found to be monoclinic

with parameters ***a*** = 5.09 Å, ***b*** = 10.88 Å, ***c*** = 27.73 Å and β=79.6°. The crystalline reflections from the hard-segment crystals of copolymer were indexed using the corresponding monomer unit cell. The latter approach allowed direct measurement of crystal orientation and phase transitions of the hard-segment crystals using simultaneous time-resolved X-ray scattering and mechanical stretching experiments. We also discovered that elastomers, which have a soft-block length of 2000 $g \cdot mol^{-1}$, crystallize upon stretching at ambient temperature. Stress-induced crystallization results in a 60 °C increase of melting temperature of PTHF crystals compared to the isotropic copolymers. Two main morphologies were observed during stretching of segmented PEEA copolymers. At low strains the polymer chains of fibril-like crystals were oriented perpendicular to the flow direction due to the crystals' high aspect ratio, whereas higher strains caused bisoxalamide crystal fragmentation and changed the preferential stem direction to the one parallel to the drawing direction. The chain tilt in the bisoxalamide crystals was deduced based on the characteristic four-spot SAXS patterns. We found that it remained constant even at high deformations. The tilting angle of the bisoxalamide unit with respect to the normal of the crystal basal plane is relatively small (i.e. between 5° and 16°) in the case of glycine end group and increases to 24° for alanine and propyl segment. The free energy of the bisoxalamide crystal surface was found to be extremely low (~18 erg/cm^2), which is likely due to the entropic contribution of the tie PTHF chains bridging neighbouring crystals. Detailed structural information, knowledge about structure formation and thermodynamics of the novel polymer materials will help to efficiently exploit them in various fields of hi-tech and medical applications.

ASSOCIATED CONTENT

Supporting Information. Measured and calculated *d*-spacing values obtained from X-ray diffraction on Gly-Oxa$_2$6-Gly monomer and oriented PTHF crystals of **2900Gly6**, optical microscopy images of the particles of Gly-Oxa$_2$2-Gly monomer and polymer **1000Gly2** on the chip active area and Nanocalorimetric cooling profiles. This material is available free of charge via the Internet at http://pubs.acs.org.

AUTHOR INFORMATION

Corresponding Authors

*E-mail: yaroslav.odarchenko@rhul.ac.uk

*E-mail: dimitri.ivanov@uha.fr

Author Contributions

All authors contributed to writing the manuscript and approved the final version of the paper.

ACKNOWLEDGMENT

The authors are grateful to Wim Bras, Giuseppe Portale and Daniel Hermida Merino from the DUBBLE beamline (ESRF, France) for fruitful discussions and excellent technical support. Y.I.O. and M.S. acknowledge the BBSRC grant BB/L018152/1. D.D. thanks the support granted by the EADS Foundation. D.A.I. and M.R. acknowledge the Russian Ministry of Science and Education for financial support (project No. 11.G34.31.0055 from 19.10.2011 and project No. 14.604.21.0079). J.J.H. thanks the IUPAC Project PAC-PAL-10-02-26.

REFERENCES

(1) Gaymans, R. J. *Prog. Polym. Sci.* **2011**, *36*, 713–748.

(2) Buckwalter, D. J.; Hudson, A. G.; Moore, R. B.; Long, T. E. *Polymer* **2014**, *63*, 1184–1191.

(3) Versteegen, R. M.; Kleppinger, R.; Sijbesma, R. P.; Meijer, E. *Macromolecules* **2006**, *39*, 772–783.

(4) Sijbrandi, N. J.; Kimenai, A. J.; Mes, E. P. C.; Broos, R.; Bar, G.; Rosenthal, M.; Odarchenko, Y.; Ivanov, D. A.; Dijkstra, P. J.; Feijen, J. *Macromolecules* **2012**, *45*, 3948–3961.

(5) Niesten, M. C. E. J. *Polymer* **2000**, *41*, 8487–8500.

(6) Niesten, M. C. E. J.; Harkema, S.; van der Heide, E.; Gaymans, R. J. *Polymer* **2001**, *42*, 1131–1142.

(7) Le Fevere de Ten Hove, C.; Penelle, J.; Ivanov, D. A.; Jonas, A. M. *Nat. Mater.* **2004**, *3*, 33–37.

(8) Ivanov, D. A.; Bar, G.; Dosière, M.; Koch, M. H. J. *Macromolecules* **2008**, *41*, 9224–9233.

(9) Ivanov, D. A.; Hocquet, S.; Dosiére, M.; Koch, M. H. J. *Eur. Phys. J. E. Soft Matter* **2004**, *13*, 363–378.

(10) Rathore, O.; Sogah, D. Y. *J. Am. Chem. Soc.* **2001**, *123*, 5231–5239.

(11) Feng, L.; Kamal, M. R. *Int. Polym. Process.* **2006**, *21*, 402–411.

(12) Zhang, F.; Liu, J.; Fu, Q.; Huang, H.; Hu, Z.; Yao, S.; Cai, X.; He, T. *J. Polym. Sci. Part B Polym. Phys.* **2002**, *40*, 813–821.

(13) Rosenthal, M. Curvy polymer crystals: why crystalline lamellae twist during growth, PhD thesis, Université de Haute Alsace, 2010.

(14) Colombe, G.; Gree, S.; Lhost, O.; Dupire, M.; Rosenthal, M.; Ivanov, D. A. *Polymer* **2011**, *52*, 5630–5643.

(15) Lin, L.; Argon, A. S. *J. Mater. Sci.* **1994**, *29*, 294–323.

(16) Yeh, F.; Hsiao, B. S.; Sauer, B. B.; Michel, S.; Siesler, H. W. *Macromolecules* **2003**, *36*, 1940–1954.

(17) Sauer, B. B.; Mclean, R. S.; Gaymans, R. J.; Niesten, M. C. J. E. *J. Polym. Sci. Part B Polym. Phys.* **2003**, *42*, 1783–1792.

(18) Bonart, R. *J. Macromol. Sci. Part B* **1968**, *2*, 115–138.

(19) Peterlin, A.; Baltá-Calleja, F. J. *Kolloid-Zeitschrift Zeitschrift für Polym.* **1970**, *242*, 1093–1102.

(20) Peterlin, A. *J. Mater. Sci.* **1971**, *6*, 490–508.

(21) Hocquet, S.; Dosie, M.; Thierry, A.; Lotz, B.; Koch, M. H. J.; Dubreuil, N.; Ivanov, D. A.; Dosière, M. *Macromolecules* **2003**, *36*, 8376–8384.

(22) Hocquet, S.; Dosiere, M.; Tanzawa, Y. *Macromolecules* **2002**, 5025–5033.

(23) Rosenthal, M.; Bar, G.; Burghammer, M.; Ivanov, D. A. *Angew. Chemie* **2011**, *123*, 9043–9047.

(24) Sijbrandi, N. J.; Kimenai, A. J.; Mes, E. P. C.; Broos, R.; Bar, G.; Rosenthal, M.; Odarchenko, Y. I.; Ivanov, D. A.; Feijen, J.; Dijkstra, P. J. *Polymer* **2012**, *53*, 4033–4044.

(25) Piazzon, N.; Rosenthal, M.; Bondar, a.; Spitzer, D.; Ivanov, D. a. *J. Phys. Chem. Solids* **2010**, *71*, 114–118.

(26) Rosenthal, M.; Doblas, D.; Hernandez, J. J.; Odarchenko, Y. I.; Burghammer, M.; Di Cola, E.; Spitzer, D.; Antipov, a E.; Aldoshin, L. S.; Ivanov, D. a. *J. Synchrotron Radiat.* **2014**, *21*, 223–228.

(27) Chatani, Y.; Ueda, Y.; Tadokoro, H.; Deits, W.; Vogl, O. *Macromolecules* **1978**, *11*, 636–638.

(28) Franco, L.; Subirana, J. A.; Puiggalí, J. *Macromolecules* **1998**, *31*, 3912–3924.

(29) Armelin, E.; Alemán, C.; Puiggali, J. *J. Org. Chem.* **2001**, *66*, 8076–8085.

(30) Cesari, M.; Perego, G.; Mazzei, A. *Die Makromol. Chemie* **1965**, *83*, 196–206.

(31) Huang, S.; Jiang, S. *RSC Adv.* **2014**, *4*, 24566.

(32) De Santis, F.; Adamovsky, S.; Titomanlio, G.; Schick, C. *Macromolecules* **2006**, *39*, 2562–2567.

(33) Kolesov, I.; Mileva, D.; Androsch, R.; Schick, C. *Polymer* **2011**, *52*, 5156–5165.

(34) Krijgsman, J.; Feijen, J.; Gaymans, R. J. **2004**, *45*, 4685–4691.

(35) Bassett, D. C. *Principles of Polymer Morphology*; Cambridge University Press: Cambridge, 1981.

(36) Ungar, G.; Keller, A. *Polymer* **1987**, *28*, 1899–1907.

(37) Barham, P. J.; Keller, A.; Otun, E. L.; Holmes, P. A. *J. Mater. Sci.* **1984**, *19*, 2781–2794.

(38) Lee, S.; Rutledge, G. C. *Macromolecules* **2011**, *44*, 3096–3108.

(39) Odarchenko, Y. I.; Sijbrandi, N. J.; Rosenthal, M.; Kimenai, a J.; Mes, E. P. C.; Broos, R.; Bar, G.; Dijkstra, P. J.; Feijen, J.; Ivanov, D. A. *Acta Biomater.* **2012**, *9*, 6143–6149.

(40) Harrison, I. R. *J. Polym. Sci. Part A-2 Polym. Phys.* **1973**, *11*, 991–1003.

(41) Hoffman, J. D.; Davis, G. T.; Lauritzen, J. I. *Treatise on Solid State Chemistry, Vol. 3*; Hannay, N. B., Ed.; Plenum Press: New York, 1975.

(42) Lee, S.; Phillips, P. *Eur. Polym. J.* **2007**, *43*, 1933–1951.

For Table of Contents use only

"Primary chemical sequence ultimately determines crystal thickness in segmented all-aliphatic co-polymers"

by

Yaroslav I. Odarchenko[a,b*], *Denis V. Anokhin*[c], *David Doblas*[a], *Martin Rosenthal*[c], *Jaime J. Hernandez*[a], *Loic Vidal*[a], *Niels J. Sijbrandi*[d], *Ad J. Kimenai*[f], *Edwin P.C. Mes*[f], *René Broos*[f], *Georg Bar*[e], *Pieter J. Dijkstra*[d], *Jan Feijen*[d], *Mikhail Soloviev*[b] *and Dimitri A. Ivanov*[a,c]*